Estimating abundance indices of juvenile fish in estuaries using Geostatistics: An example of European sea bass (Dicentrarchus labrax)

Amédée Roy, Christophe Lebigre, Mickaël Drogou, Mathieu Woillez

Version of Record: https://www.sciencedirect.com/science/article/pii/S0272771422000580
Manuscript_8974a208523f93151ca57b213a78f611

ESTIMATING ABUNDANCE INDICES OF JUVENILE FISH IN ESTUARIES USING GEOSTATISTICS: AN EXAMPLE OF EUROPEAN SEA BASS (*Dicentrarchus labrax*)

Amédée Roy
DECOD (Ecosystem Dynamics and Sustainability),
IFREMER, INRAE, Institut Agro,
Plouzané, France
amedee.roy@ifremer.fr

Christophe Lebigre
DECOD (Ecosystem Dynamics and Sustainability),
IFREMER, INRAE, Institut Agro,
Plouzané, France
christophe.lebigre@ifremer.fr

Mickaël Drogou
DECOD (Ecosystem Dynamics and Sustainability),
IFREMER, INRAE, Institut Agro,
Plouzané, France
mickael.drogou@ifremer.fr

Mathieu Woillez
DECOD (Ecosystem Dynamics and Sustainability),
IFREMER, INRAE, Institut Agro,
Plouzané, France
mathieu.woillez@ifremer.fr

January 30, 2022

ABSTRACT

Estuaries play a fundamental role in the renewal of fisheries resources, as they hold nurseries for many juvenile fish species. Estimating juveniles' abundance in estuaries is therefore key to improve stock assessment models, anticipate future recruitment and prevent crises related to biomass collapse. While geostatistical methods have been widely used in fisheries science to estimate species' abundance during offshore scientific surveys, difficulties arise when using these methods in estuaries. Indeed, these ecosystems are characterized by their irregular and often non-convex morphology, their environmental gradients (salinity, depth), and their tidal dynamics which question the validity of the hypothesis of second-order stationarity, fundamental to the theory of intrinsic geostatistics. Therefore, we tested the performance of different geostatistical methods to account for the complexity of these ecosystems and quantify robust indices of abundance adapted to estuaries. We used density data of juvenile sea bass (*Dicentrarchus labrax*) sampled with demersal trawls in the Loire River collected over three consecutive years and tested a metric space for which the distance along the estuary is considered. We took into account the non-stationarity of densities with either a transitive approach or an intrinsic approach with spatio-temporal external drifts, which takes into account the effects of tides and environmental gradients. These geostatistical methods allowed us to produce densities distribution maps and had substantially greater predictive capabilities than the stratified random

estimator (classical reference estimator). However, geostatistical methods consistently had larger CVs than the stratified random estimator because the latter ignores the spatio-temporal distribution of sampling points leading to uncertainties underestimates and hence overly optimistic confidence intervals. The use of geostatistically computed abundance indices in an assessment model appears to be a conservative approach, whose uncertainties would allow a more robust adjustment trade-off between different indices when estimating recruitment in estuaries.

***K*eywords** Pre-recruitment indices · Transitive Kriging · Intrinsic Kriging · Kriging with External Drift · Tidal Dynamics · Seabass

1 Introduction

Estuaries are important areas for the early life history of many marine organisms: each year larval fishes are recruited into estuarine habitats in which they grow to juveniles' stages over several years before moving to adult habitats offshore [1, 2]. Indeed, estuaries usually offer areas of shallow waters with high food availability, and low predation pressure [3]. Thus, the role of these productive ecosystems as nurseries is an established ecological concept: a nursery being any habitat that makes a greater than average contribution to the recruitment of adults [4, 5]. These areas are therefore particularly interesting for estimating indices of juvenile's abundance. Several studies have been dedicated to the estimation of abundance, growth, and mortality of larvae or juvenile fish in estuaries from scientific surveys providing crucial information for fisheries stock evaluation and management [6, 7, 8].

The determination of indices of abundance and associated uncertainties from fish surveys is however a classical challenge in fishery science. Among the existing methods for estimating indices, classical approaches are often based on random sampling theory such as the stratified random estimator [9]. This method generally calculate average catches in predetermined sampling stratum, and define the total abundance as the area-weighted sum of stratum abundances [10]. However, the abundance indices estimated using this approach are produced without any assumptions about the spatial distribution of the population. To account for the spatial dependence of samples, geostatistical methods have therefore been used to estimate fish abundance since the early 1990s [11]. The purpose of geostatistics is thus to estimate and model the spatial structure of dependence, to extrapolate the studied variables at unknown locations [12], which enables the estimation of abundance indices and associated variance [13]. Hence, numerous studies have shown that taking spatial correlation into account when processing survey data yielded to more precise and accurate indices of abundance [14, 15].

However, the estimation of auto-correlation structures is often difficult in practice because of fish movements and variations in their aggregative behaviour [16]. Indeed, the sampling of fish densities through a whole domain requires a certain amount of time, and space-time variations of fish density occurring between two samplings can affect the data in various ways [13]. Specifically, estuaries are particularly complex ecosystems characterized by substantial environmental gradients (topography, salinity, temperature), and tidal dynamics (current velocity, sea level). Numerous

studies have indeed reported fish movements and variations of their habitat distribution in relation to tidal cycles, particularly for pelagic juveniles [17, 18, 19]. Moreover most estuaries are also irregularly-shaped non-convex domains, and the use of euclidean distance may not be appropriate for the analysis of their spatial structures' dependence [20, 21]. The observation of spatial auto-correlation in estuarine domains yields therefore to several challenges and it is crucial to understand the physical nature of estuaries, and the environmental preferendum of the studied juvenile fishes to produce relevant abundance indices [22].

European sea bass (*Dicentrarchus labrax*) is a highly exploited demersal fish from the North East Atlantic with a partially migratory behaviour [23]. Sea bass wild populations have recently declined substantially, with catches from the northern sea bass stock (ICES divisions IV.b-c, VII.a and VII.d-h) dropping from about 4000 tonnes in years 2005-2013 to about 1000 tonnes from 2015 onwards [24, 25]. From their first summer up to age 2 to 5 depending on habitat characteristics, immature sea bass inhabit coastal nursery areas such as estuaries, with a reported preferendum for shallow waters with relatively high turbidity and low salinity [26, 27]. A high local site fidelity has been observed, with juveniles staying for longer periods in proximity of the same nursery areas [28], and migrating daily between subtidal and intertidal habitats [29]. Such behaviour points out the highly non-stationarity of estuarine domains in terms of space and time, which is likely to bring substantial variance in trawling samples and making it difficult to estimate accurately spatial covariance structures.

Geostatistics offers a very flexible framework and a wide range of geostatistical methods have been used for fisheries stock assessment [13, 30]. Generally, studies have adopted the so called 'intrinsic approach' which is based on the theory of random fields and relies on stationary hypothesis. Hence this approach includes (i) cokriging, where kriging is extended to the multivariate case [31, 32], (ii) external drift kriging, which enables to take into account external variables when they are known in the whole studied domain [33, 34], (iii) conditional simulations, particularly interesting for combining data with different sources of variability [35], and many other variants [30]. Transitive kriging has also been introduced to fisheries as an alternative to the intrinsic theory for global estimation which requires fewer hypotheses, when stationary hypotheses are not relevant (e.g. in highly variable environment drifted by complex oceanographical processes) [16].

The aim of this study was therefore to identify the most relevant geostatistical method for the estimation of juvenile sea bass abundance in an estuarine domain, and to quantify performance over the random stratified estimator. The first part of this manuscript is a recall of main geostatistical theories, including intrinsic and transitive geostatistics. Then we compared a total 6 geostatistical methods for estimating sea bass juveniles abundance in the estuary of Loire (France) for three consecutive years. In particular, we focused on assessing the impact of the estuary's morphology, environmental gradients, and tidal dynamics on the estimation of abundance indices. Finally, we provide a few recommendations concerning the estimation of juvenile abundance indices in estuaries to highlight the value of this particularly valuable information in stock assessment models.

2 Geostatistical theory

Geostatistics is a relevant method for the estimation of the total abundance Q of a regionalized variable $z(x)$ (e.g. fish density) within a domain D from a collection of samples $z(x_i)$. It consists in a four step process where (i) we collect fish density samples and any relevant environmental covariates (sampling step), (ii) we evaluate and model the way the spatial data $z(x)$ is coregionalized (variography step), (iii) we estimate the studied variable z at unknown locations as a linear combination of known samples $z(x_i)$ (kriging step), (iv) we estimate the mean and variance of the studied variable over the whole domain D (abundance index estimation step; Fig. 1). The following section recalls the basics of geostatistical theory both for intrinsic and transitive approaches. The reader might want to refer to [12] for further details and explanations.

2.1 Intrinsic Approach

Variography

The fundamental premise of intrinsic geostatistics is that collected spatial data $z(x)$ are a realization of a random field Z. By assuming that there is no systematic variation underlying such random field, the expectation of $Z(x)$ is supposed to be independent of the position (i.e. $\mathbb{E}[Z(x)] = m$); this is the first order stationarity hypothesis where m represents the expectation of the random variable $Z(x)$, which does not necessarily equal the mean of one random field realization. Then, by assuming that the variance is also independent of the position (i.e. $\mathbb{E}[Z(x)^2] = \sigma^2$), we can express the covariance of the regionalized variable through the variogram $\gamma(h)$, where h is the distance between two locations of the domain (Eq. 1) ; this is the second order stationarity hypothesis.

$$\begin{aligned} \text{cov}[Z(x+h), Z(x)] &= \mathbb{E}[(Z(x+h) - m)(Z(x) - m)] \qquad \text{with } \mathbb{E}[Z(x)] = m \\ &= \sigma^2 - \frac{1}{2}\mathbb{E}[(Z(x+h) - Z(x))^2] \qquad \text{with } \mathbb{E}[Z(x)^2] = \sigma^2 \\ &= \sigma^2 - \gamma(h) \end{aligned} \tag{1}$$

In short, based on stationarity assumptions, the intrinsic formalism describes the structural auto-correlation of the field $Z(x)$ within D as a function of the distance : the variogram. A variogram therefore represents the way a regionalized variable is spatially structured, and captures its intrinsic behavior. In practice, experimental variograms are estimated from sampling values using usually the following formula:

$$\gamma^*(h) = \frac{1}{2N(h)} \sum_{i=1}^{N(h)} (z(x_i + h) - z(x_i))^2 \tag{2}$$

Where $N(h)$ is the number of experimental pairs of data $(z(x_i), z(x_i + h))$. They are then fitted with a variogram model γ to which we will refer in following sections [36].

Ordinary Kriging (OK)

Ordinary Kriging (OK) allows to estimate the fish density at a unknown location $Z(x_0)$ from observed densities $Z(x_i)$. It is defined as the best linear unbiased estimator of $Z(x_0)$ (i.e. it is a linear combination of known data values) which weights are defined such that the estimator minimizes the error in the variance estimation. The estimator is thus written $Z^*(x_0) = \sum_i w_i Z(x_i)$, with kriging weights satisfying $\sum_i w_i = 1$, as the first-order stationarity assumption implies a constant mean. The variance of the estimator can finally be expressed through the intrinsic covariance function (Eq. 3).

$$\begin{aligned} \text{var}(Z^*(x_0) - Z(x_0)) &= \mathbb{E}[(Z^*(x_0) - Z(x_0))^2] \\ &= \mathbb{E}[(\sum_i w_i Z(x_i) - Z(x_0))^2] \\ &= \sum_i \sum_j w_i w_j \gamma(x_i - x_j) - \sum_i w_i \gamma(x_i - x_0) \end{aligned} \tag{3}$$

Minimizing the error variance under the constraint on the weights and using the method of Lagrange multipliers leads to a linear system to be solved for the kriging weights (Eq. 4). This system is composed of $n + 1$ equations where n is the number of samples, and μ is the Lagrange parameter.

$$\begin{cases} \sum_i w_i \gamma(x_i - x_j) + \mu = \gamma(x_i - x_0) \text{ for } j = 1, ..., n \\ \sum_i w_i = 1 \end{cases} \tag{4}$$

Kriging with External Drift (KED)

In order to account for underlying systematic drift of the field, kriging with an External Drift (KED) assumes that the mean of the process is linearly related to any external variable(s) known in the whole studied domain (Eq. 5). In the situation where the mean of the process depends on a function of time t and space x we have:

$$\mathbb{E}[Z(x,t)] = m(x,t) = a + bf(x,t) \tag{5}$$

The framework is similar to that of OK, and Eq. 3 holds. Yet in this situation, the conditions on linear estimators becomes:

$$\sum_i w_i = 1 \text{ and } \sum_i w_i f(x_i, t_i) = f(x_0, t_0) \tag{6}$$

The kriging weights are once again obtained by minimizing the variance of the estimation error, leading to the following linear system, where μ_0 and μ_1 are the Lagrange parameters:

$$\begin{cases} \sum_i w_i \gamma(x_i - x_j, t_i - t_j) + \mu_0 + \mu_1 f(x_i, t_i) = \gamma(x_i - x_0, t_i - t_0) \text{ for } j = 1, ..., n \\ \sum_i w_i = 1 \\ \sum_i w_i f(x_i, t_i) = f(x_0, t_0) \end{cases} \tag{7}$$

In this approach, the estimation of a fish density at an unknown location and time depends therefore on the auto-correlation structure defined by the model γ, but also modulates according to the value of the external variable f. The difference between OK and KED are schematically illustrated in Fig. 1.

Abundance Index estimation

For both OK and KED, the estimation of the total abundance $Z(D)$ over the whole studied domain D consists in averaging kriged densities at every locations of the domain: $Q^* = Z(D) = \sum_{x_k \in D} Z(x_k)$. However, for KED the use of a temporal drift allows the mean of the process Z to vary in time (Eq. 5). The estimation of the total abundance for KED is therefore performed at a fixed time, and hence the weights are modulated according to timing of samples' collection [37]. The associated estimation's variance is not however the average of kriging variances but can be computed from the covariance model γ, the domain D, and the computed weights w_i as follow:

$$\begin{aligned} \sigma_E^2 &= \mathbb{E}[Z(D) - Z^*(D)]^2 \\ &= \mathbb{E}[Z(D) - \sum_i w_i Z(x_i)]^2 \\ &= -\bar{\gamma}(D, D) + 2 \sum_i w_i \bar{\gamma}(x_i, D) - \sum_i \sum_j w_i w_j \gamma(x_i - x_j) \end{aligned} \tag{8}$$

Where $\bar{\gamma}(D, x_i)$ represents the mean value of the variogram γ with point x describing the whole domain D. This equation holds for both OK and KED at fixed time.

2.2 Transitive Approach

The estimation of variograms is often difficult in practice because of the characteristics of fish survey data (i.e., numerous low or zero densities, clear location of a few high density values in the field) and because of the stationary hypotheses associated [12, 13, 16]. The Transitive Approach has been introduced to fisheries as an alternative to the intrinsic theory for global estimation when dealing with regular sampling. It is known to be more robust than the intrinsic approach, though it has not been widely used in fisheries science. This method is indeed less flexible as it cannot take into account spatial nor any temporal covariables [13].

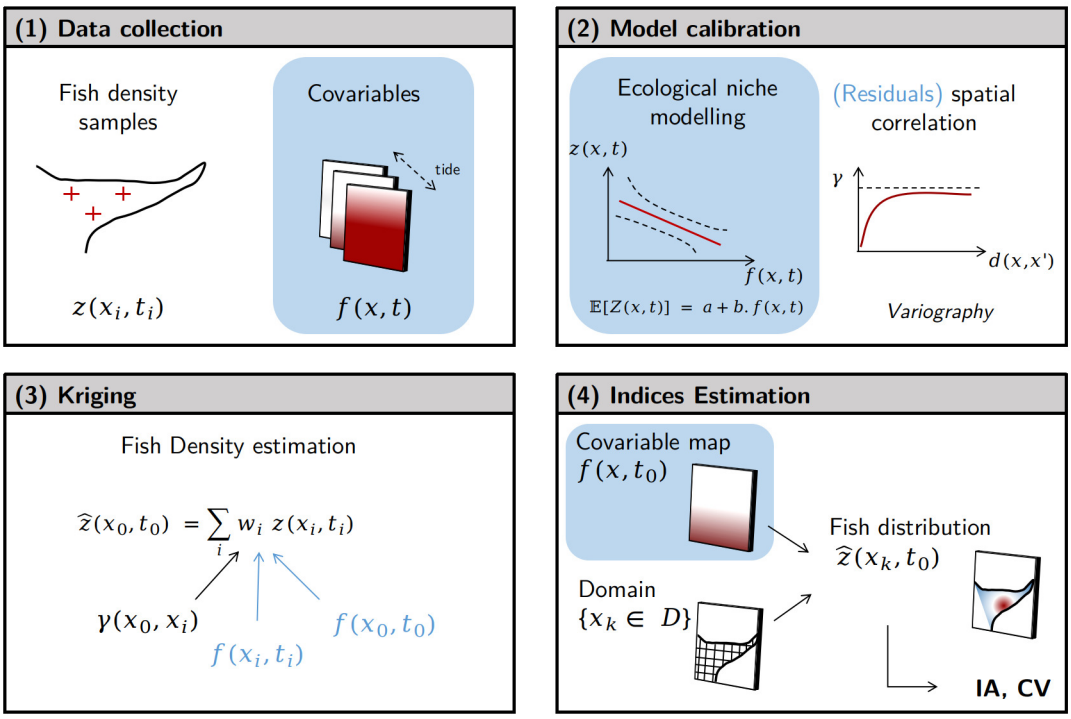

Figure 1: Framework for abundance indices estimation using geostatistical tools. Geostatistical tools are used to estimate abundance indices from a set of regionalized density samples (1) and are based on a description of its auto-correlation structure (2). This model is then used for estimating densities at unknown locations (3) and thus for deriving relevant indices (4). Spatio-temporal covariates can also be used as external drift (in blue); this enables the account for the dynamics of the covariable when estimating a fish density at an unknown location (3). On the counterpart, the abundance indices estimated using a temporal drift depend on the estimation time t_0 (4).

Transitive covariogram

In this approach, the regionalized variable is described by the transitive covariogram. This has some similarity with an intrinsic variogram, however it is not an expectation but a sum, making transitive covariograms particularly robust to outliers [30].

$$g(h) = \int z(x)z(x+h)dx \tag{9}$$

The covariogram decreases from its maximum value and stabilizes at 0 at a distance corresponding to size of the area in which the focal population is present (i.e. its range).

Transitive Kriging (TR)

Kriging can also be performed in the transitive approach, to predict a density at unknown location as a weighted average of sampled locations.

$$z^*(x) = \sum_i w_i z(x + h_i) = \sum_i w_i z(x_i) \tag{10}$$

Weights w_i are then estimated by minimizing the sum of squared errors between real and estimated densities when translating positions x and $x + h_i$ over space with the same relative geometrical configuration (Eq. 11)).

$$\begin{aligned} \int (z(x) - z^*(x))^2 dx &= \int (z(x) - \sum_i z(x + h_i))^2 dx \\ &= g(0) - 2\sum_i w_i g(h_i) + \sum_i \sum_j g(h_i - h_j) \end{aligned} \tag{11}$$

Where g is the covariogram defined in Eq. 9. The estimation of kriging weights thus consists in solving a linear system, similarly to intrinsic kriging, but using the transitive covariogram instead of the covariance variogram.

Abundance index estimation

From regular sampling grid with regular mesh surface the unbiased estimator of the total abundance is defined as the sum of the sample values multiplied by the surface of the grid mesh (Eqs in 1D):

$$Q(X_0)^* = s \sum_k z(X_0 + ks) \tag{12}$$

where X_0 is the origin of the grid mesh seen as a random variable uniformly distributed all over the studied area. The estimation variance can therefore be computed as:

$$\begin{aligned} \sigma^2_{est} &= \mathbb{E}[(Q^*(X_0) - Q)^2] \\ &= \int_s (s \sum_k z(x + ks) - Q)^2 \frac{dx}{s} \\ &= \int_s s \sum_{k,l} z(x + ks) z(x + ls) - 2Q \sum_k z(x + ks) + Q^2 dx \\ &= \sum_k \sum_l s \int_s z(x + ks) z(x + ls) dx - Q^2 \\ &= s \sum_k g(ks) - \int g(h) dh \end{aligned} \tag{13}$$

Hence, the major assumption of the transitive approach is the randomness of the origin of the sampling grid. This approach therefore differs fundamentally from the intrinsic geostatistical approach in which the stochastic part of the model concerns the density seen as the realization of a random field. In this sense, the transitive approach relies on fewer hypotheses and enables the estimation of the total abundance and variance from regular sampling data, based on a model of $g(h)$ and on the grid mesh interval s. The framework can be extended when the sample grid is not strictly regular, the experimental computation of the covariogram has to be weighted by the area of influence of each datapoint.

3 Material and Methods

3.1 NOURDEM Survey Data

The NOURDEM survey is conducted by the laboratory of fisheries biology of Ifremer (Plouzané, France) and aims at establishing index of demersal fish juveniles' abundance in nurseries. Three surveys have been carried out in three consecutive years in the Loire estuary (Fig. 2): from 2016-06-09 to 2016-06-16, from 2017-06-29 to 2017-07-06 and from 2018-07-03 to 2018-07-10 [38]. This survey follows strictly pre-defined sampling procedures [39]. Sampling locations have been designed homogeneously in the estuary covering all brackish waters with water salinity from 0 to 35. The 46 trawling stations are represented in Fig. 2. For each survey, all stations have been sampled at least once, and ca. 60% of the trawling stations have been sampled twice, particularly in waters with low salinity were the highest fish densities were expected. All samples were collected using a fishing vessel with a small large vertical opening trawl specifically designed to catch demersal fish juveniles. For each trawl, the boat went against the current at ca. 1450 engine rpm, during 15 minutes. At the end of each trawl, the entire catch was systematically weighed, all species were identified and sorted. Then all or some of the individuals of each fish species were measured. For very heavy trawl loads, weighing and measurement were only carried out on a random subset of the trawls' total weight. Trawl depth, salinity, and temperature were measured directly for every sampling. For sea bass, age were estimated based on annual increment fish scale readings. A minimum of 3 age readings were performed per length classes, i.e. cm. For this study we focused on the spatial distribution of G2-aged sea bass, as this age group is well sampled by the survey. Ages have been determined by fixing arbitrary thresholds with respect to the modes appearing in the age-length keys distribution of captured fishes (see Annex). Such distribution and associated threshold are illustrated in Fig. 3.

3.2 Estimating abundance indices in Loire's estuary

The usual ordinary kriging approach relies on the stationarity hypothesis, yet the strong environmental gradient and dynamics characterizing estuaries are likely to call this hypothesis into question. We therefore investigated two alternatives to ordinary kriging either (i) staying within the intrinsic approach but to take into account the non-stationarity through the use of a drift (e.g. kriging with external drift), or (ii) by doing no assumptions on stationarity through a transitive approach. In addition to these direct approaches we also investigated kriging in a projected metric space for which the distance along the estuary is considered to take into account the convex nature of the Loire estuary.

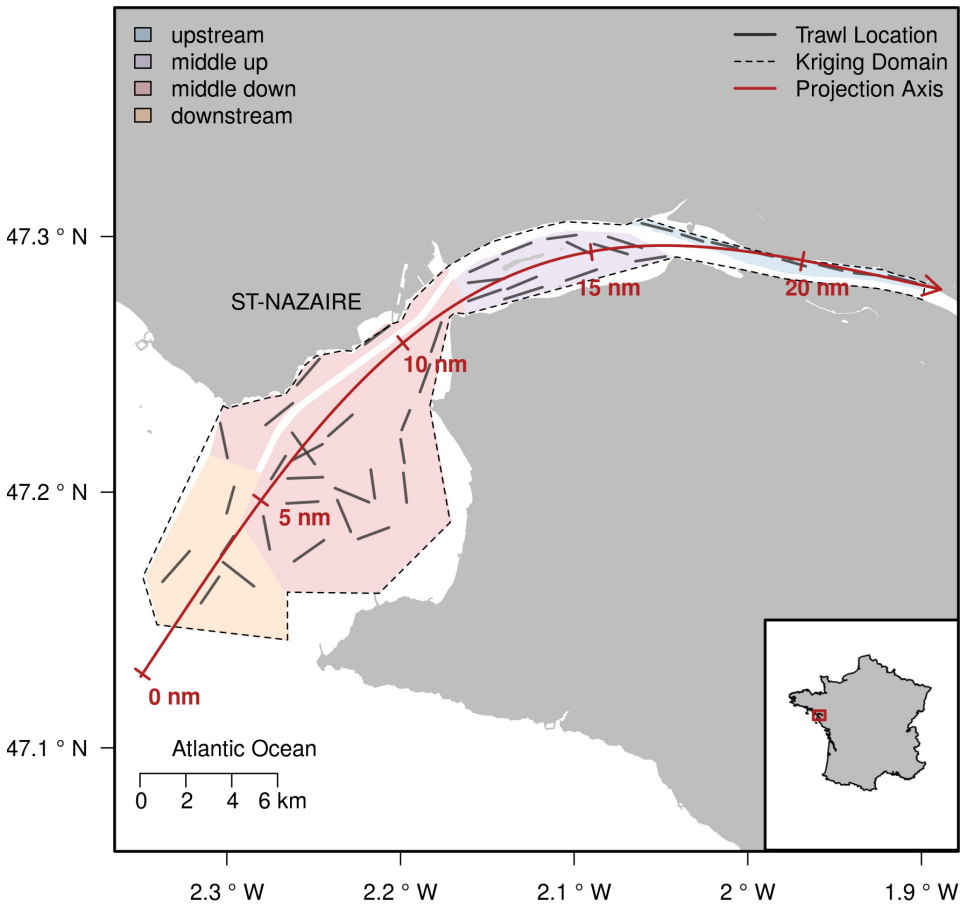

Figure 2: Map of the Loire's estuary. Coloured areas referred to stratas detailed in Table 1 and used for random sampling estimations. The red line illustrates the axis and associated scale used for the channel-centered projection. The scale is given in nautical miles (nm) along the projection axis.

Therefore, we overall tested the 6 following methods on each yearly dataset: Ordinary kriging (OK), projected Ordinary Kriging (OKp), Kriging with External Drift (KED), projected Kriging with an External Drift (KEDp), Transitive kriging (TR), and Projected Transitive kriging (TRp). This section aims at detailing the framework followed for each of these approaches.

3.2.1 Projection

The Loire's estuarine domain is non-convex (i.e. the line segment connecting two points within the estuary may intercept land) which could possibly lead to misinterpretation of spatial covariance structures based upon simple Euclidean distance metric. We therefore performed a channel-centered coordinate transformation along the channel's centerline 2 and a transverse axis orthogonal to the centerline.

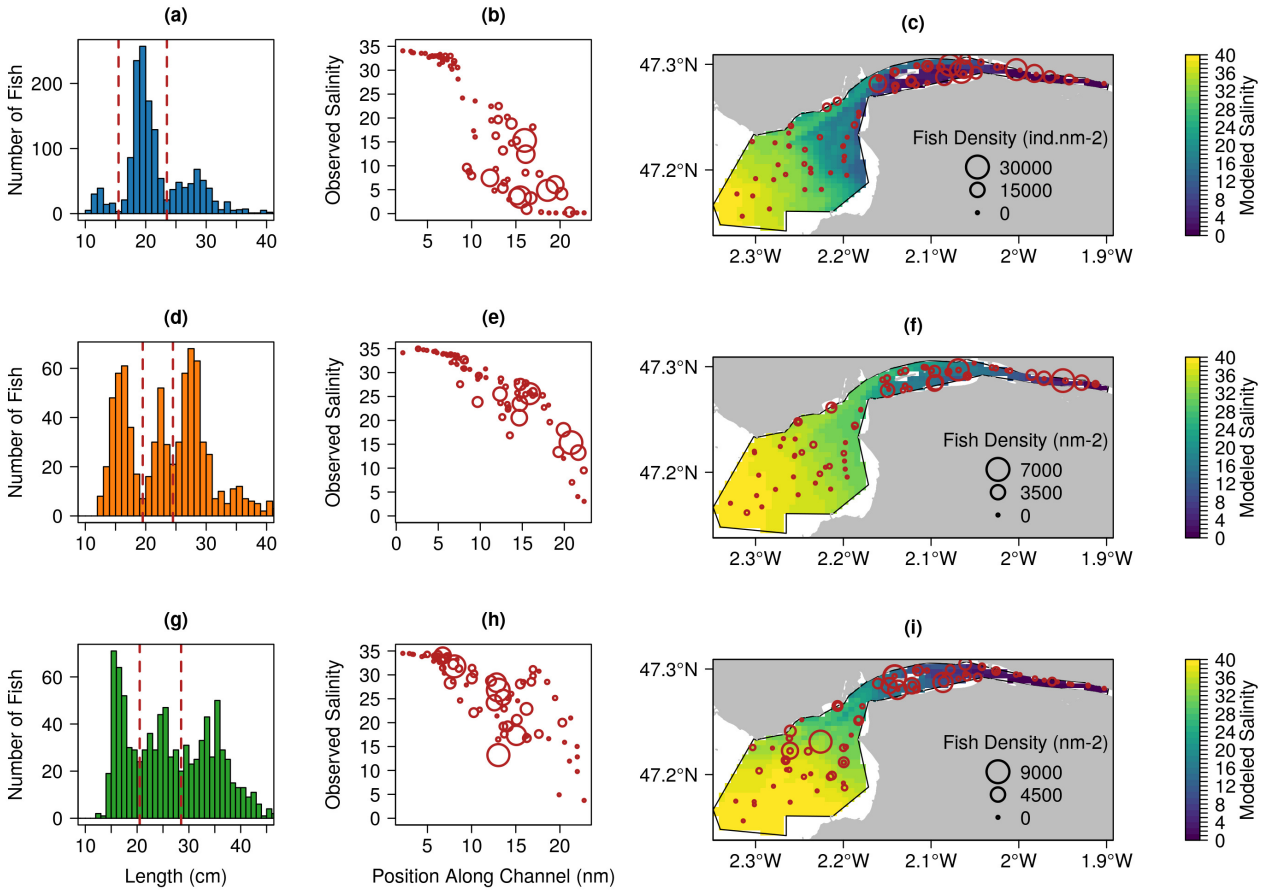

Figure 3: Data Overview: Left-column figures (a), (d) and (g) illustrate the number of captured sea bass according to their length and the thresholds used for defining G2-aged class for year 2016, 2017, and 2018 respectively. Center-column figures (b), (e) and (h) show the relationship between G2-aged sea bass densities depending on position in the estuary along the projection axis (see Fig. 2) and on salinity in 2016, 2017 and 2018. Red circles are proportional to fish density values. Maps (c), (f) and (i) represent how these fish densities are organized in space, and over a salinity map derived from MARS3D-AGRIF data for datetime 2016-06-14 10:00:00 GMT, 2017-07-02 13:00:00 GMT, and 2018-07-03 17:00:00 GMT respectively

3.2.2 Intrinsic Approach

Variography The estimation of intrinsic variography is difficult, particularly when some trawling station are doubled as it adds substantial short range variability (i.e. the nugget effect). The observation of anisotropy of fish school structures in a narrow estuary is also notably challenging. Thus, assuming that the important catch differences at identical or nearby locations may be due to tidal dynamics, we computed isotropic variograms with pairs of samples that occured at similar sea surface height anomalies. More precisely, we computed the observed sea surface height anomalies (SSHa) as the difference in space and time between the theoretical bathymetry at the sampling location and the observed depth of the trawl. Pairs of sample were used for estimating the variogram only if their differences in SSHa were lower than 5m. In other words, we performed an horizontal 3D variogram with a bench of 5 meters [40, 41], where the third dimension is the observed SSHa. The lag parameter was fixed to 0.5 nautical miles (nm), and the maximum number of lags was fixed to 11. The covariance structure used to fit empirical variograms was a combination

of a nugget and a spherical effect. This consists in a parametrized model defined by three parameters (two sills and one range). Ranges were fixed by visual inspection and sills determined with the automatic procedure provided by the RGeostat R package [42] using the algorithm presented in [43].

External drifts According to juveniles' sea bass habitat preferendum three external covariables were taken into consideration as external drifts : SSHa, salinity, and temperature [26, 27, 29]. We measured these covariables *in situ* and used them to linearly model fish densities at the sampling locations. We tested different linear models with various variable combinations and polynomial degrees and selected the most relevant parametric relations using the BIC criterion (see Table 2). We obtained maps of salinity, temperature and bathymetry from the MARS3D-AGRIF hydrodynamic database which is built with the MARS3D model along the French coast at high spatial (500m) and temporal (1h) resolution [44]. An example of used drift is shown in Fig. 3. We adjusted these model-based maps to the observed values of temperature and salinity by fitting a simple polynomial regression of degree 3, so that the mean squared error between predicted and observed values would be minimal. These adjusted maps were directly used as spatio-temporal drifts $f(x,t)$. Finally, we estimated indices following the framework given in Fig. 1. Spatial correlation structures were described from the residual of the selected models of fish densities. Indices were computed using fixed covariable maps given for mid-tide.

Table 1: Datasets Overview

Date	Strata	Surface (nm^2)	Nb of Station	Nb of Trawls	Mean $\pm$ Std G2 Density (x10^3 nm^{-2})	Max G2 Density (x10^3 nm^{-2})	Zeros	Mean Salinity	Mean Temperature (°C)	Mean Depth (m)
2016	upstream	2.1	8	14	6.0 ± 8.0	26.2	43 %	3.1	19.1	5.2
	middle up	5.5	12	23	8.7 ± 9.6	32.7	0 %	11.9	17.9	5.4
	middle down	26.7	21	31	0.8 ± 1.8	0.7	52 %	15.2	17.4	6.7
	downstream	9.9	5	5	0.0 ± 0.0	0.0	100 %	33.78	13.5	15.7
	Total	44.2	46	73	4.2 ± 7.4	32.7	37 %	12.8	17.4	7.5
2017	upstream	2.1	8	14	1.5 ± 2.2	7.3	36 %	15.1	21.3	5.2
	middle up	5.5	12	22	1.2 ± 1.4	5.4	5 %	24.8	19.6	5.1
	middle down	26.7	21	31	0.2 ± 0.4	1.8	71 %	32.0	17.6	7.2
	downstream	9.9	5	5	0.1 ± 1.5	0.3	80 %	34.8	15.3	16.1
	Total	44.2	46	72	0.7 ± 1.3	7.3	44 %	26.7	18.8	6.8
2018	upstream	2.1	8	17	0.5 ± 0.8	2.7	59 %	18.7	22.0	4.4
	middle up	5.5	12	22	2.4 ± 2.6	8.9	14 %	22.6	21.0	4.1
	middle down	26.7	21	32	1.0 ± 1.4	7.0	28 %	31.5	19.0	5.8
	downstream	9.9	5	5	0.1 ± 0.3	0.7	80 %	34.4	17.6	14.9
	Total	44.2	46	76	1.3 ± 1.9	8.9	34 %	26.2	20.1	5.6

3.2.3 Transitive Approach

Transitive Kriging has been performed as detailed in [30]. The covariograms were estimated and weighted by the area of influence of each data point. Anisotropy was estimated (i.e. covariogram estimation for specific directions; here 0°/ 90 °) both for TR with projection (along channel / orthogonal to channel) and without projection. The lag parameter was fixed to 1.5 nm which is approximately the size of the mean distance between the closest sampling locations, and

the maximal lag has been set to 20 nm so that the entire area of presence is covered. Similarly to intrinsic approach, we adjusted the empirical covariograms with a combination of nugget effect and spherical. Ranges were defined by visual inspection, and sills were fitted automatically.

3.2.4 Random Sampling Approach

For comparison, we evaluate abundance indices with a random sampling technique; the random stratified estimator (RS). To this end, we defined empirically 4 stratum within the Loire's estuary assuming that habitat were relatively homogeneous in each of these stratum (Fig. 2). Abundance indices (AI) and coefficients of variation (CVs) are thus computed as weighted sums of each stratum abundance and variance. Equations are detailed in Ifremer survey reports [39, 38].

3.3 Method Comparison

To compare geostatistical methods, we aimed at describing the robustness of spatial structure estimations by computing their goodness of fit. We used Root Mean square error (RMSE) between the normalized empirical variograms and the fitted structural models. Concerning kriging, we evaluated all methods over the same domain and with the same regular grid (mesh of 0.27 nm). This grid consisted in the grid used for the MARS3D-AGRIF hydrodynamic database delimited by the polygon presented in Fig. 2. AI and CVs have been computed following equations given above. We evaluated each method's performance using cross-validations, consisting in estimating successively each data point from other data points. We then extracted the RMSE to assess the performance of each method; the best method is the one with the smallest RMSE score.

4 Results

The three surveys carried out in 2016, 2017, and 2018 led to important differences with maximal fish densities ranging from up to 32.7e3 ind.nm^{-2} in 2016 to less than 8.9e3 ind.nm^{-2} both in 2017 and 2018 (Table 1). In particular, in 2017 the overall mean fish density was the lowest with 7e2 ind.nm^{-2} and 44% of the stations contained no G2-aged sea bass. The 'middle-up' part of the estuary (purple area in Fig. 2) was however the area where the probability to observe G2-aged sea bass was the greatest with the lowest rate of zeros for three consecutive years (respectively 100%, 95% and 86% of non-empty trawls in 2016, 2017 and 2018). Mean length of G2-aged sea bass revealed also important inter-annual variability with 20, 22.5, and 25 cm in 2016, 2017 and 2018, respectively.

Environmental conditions were substantially different from one year to another with a particular high river flow in 2016 (1,970 m^3/s in june 2016) associated to very low salinity with 12.8 in 2016 in opposition to 26.7 and 26.2 in 2017 and 2018 (see Table 1). The relationship between G2-aged juvenile sea bass densities and environmental variables depended also of the year and was better described by salinity in 2016 and 2017 (preferendum for relatively low salinity (5 to 15) in 2016; preferendum for higher salinity in 2017 (10 to 25)), whereas in 2018 the best model contained only the depth

variable (greater densities were found at lower depths; Table 2 and Fig. 4). Salinity over the estuaries depends however on the tide, and in 2016 and 2017 upstream fish densities were lower when the tide was also low (i.e. at lower salinity for a fixed position), while in the middle of the estuary fish densities were a bit higher at high tide (i.e. at higher salinity for a fixed position) (see Fig.3 for 2016 and in annex for years 2017 and 2018).

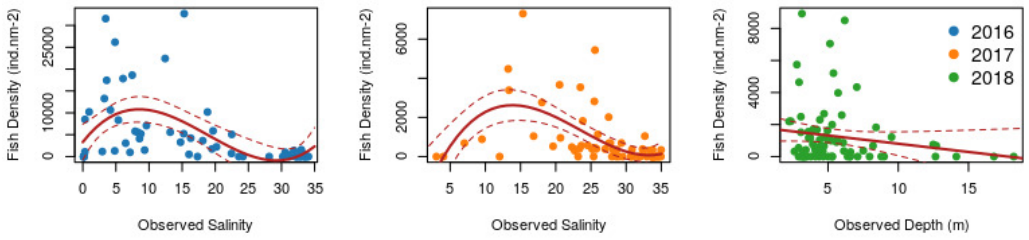

Figure 4: Prediction of the linear models selected for KED. Associated BIC and R-squared values are given in Table 2

Table 2: Overview of the linear models explored for drift selection. These linear models aimed at predicting juvenile sea bass density from different variable sets. Models finally selected for KED consisted in models with lowest BIC criterian and are described with a (*).

Year	Variables	R-squared	BIC
2016	sal	0.18	1503
	temp	0.16	1505
	depth	0.08	1511
	sal + temp + depth	0.17	1510
	sal + sal^2 + sal^3 (*)	0.29	1499
2017	sal	0.14	1245
	temp	0.16	1244
	depth	0.06	1251
	sal + temp + depth	0.14	1251
	sal + sal^2 + sal^3 (*)	0.32	1234
2018	sal	0.00	1375
	temp	0.00	1374
	depth (*)	0.02	1373
	sal + temp + depth	0.00	1381
	sal + sal^2 + sal^3	0.02	1379

Regarding the variography, adjusted structures were relatively similar over the years, all of them consisting in a combination of a nugget effect and a spherical model (see Table 3 in annex and Fig. 5). On average, transitive covariograms were easier to fit with an average goodness of fit (GOF) of ca. 0.65, which was slightly improved by the projections (GOF of 0.28). In opposition, intrinsic variograms had an averaged GOF of 2.03 caused by high variability in the first steps. For intrinsic approaches (i.e. ordinary kriging and kriging with external drift), the computation of classical variograms did not capture any spatial structures, while the use of sea surface height anomaly as a third dimension in the so-called '3D Horizontal' variogram enabled the estimation of 2 nm ranging structures (see Fig. 5). These structures were however 5 to 10 times smaller than those captured by transitive covariograms. Transitive covariograms capture indeed the structure of fish preferendum habitat and decrease from their maximum value and

stabilize at 0 at a range distance corresponding to the size of the presence area (around 15 nm). Conversely, intrinsic variograms capture the fish schooling clusters structure at a range smaller than half the length of studied area (around 6 nm).

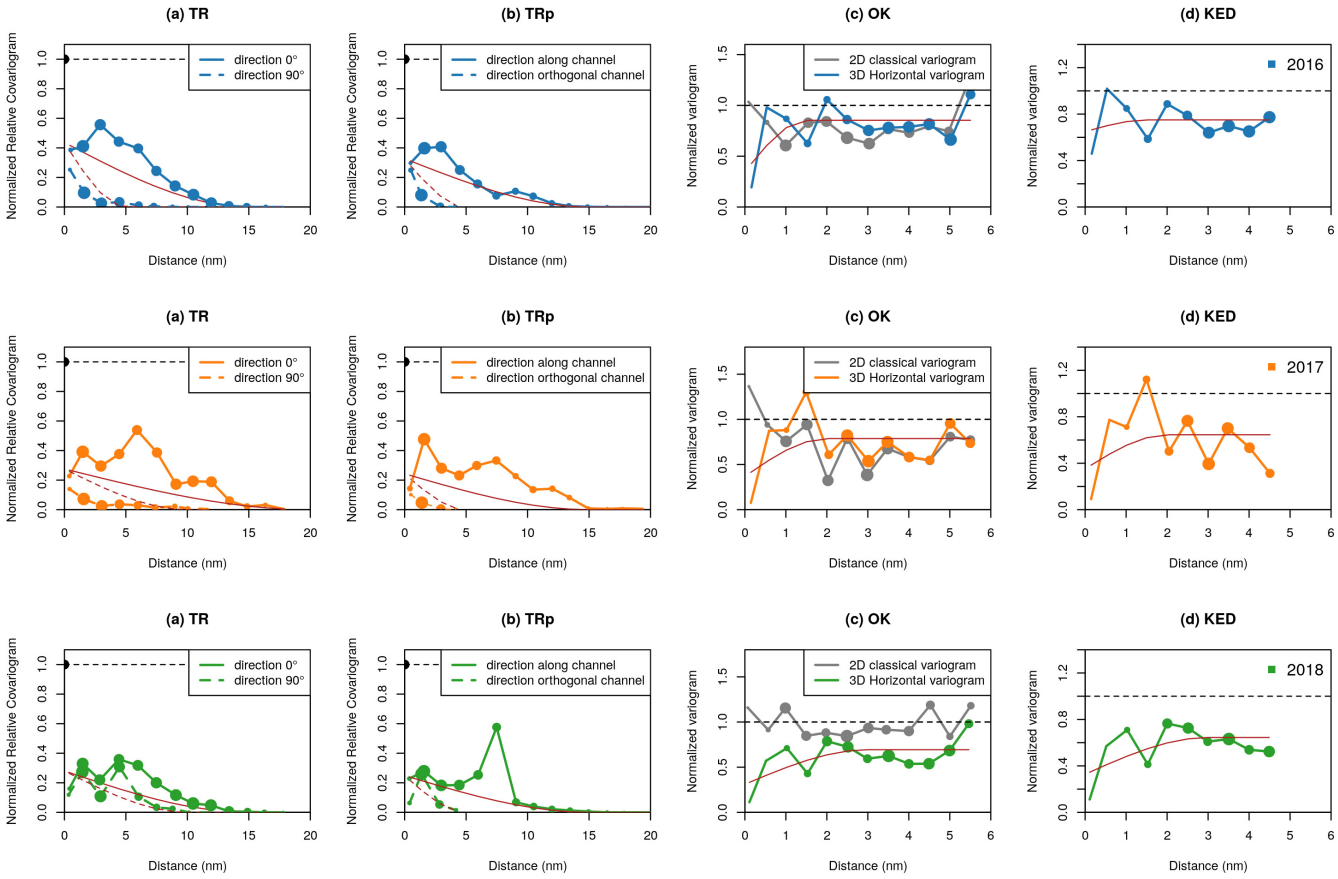

Figure 5: Variograms and fitted models for each surveys. Transitive approaches (TR and TRp were modelled using an anisotropy and covariograms describe two directional structure. Fitted model on both directions are given in filled and dotted red lines. For intrinsic approches (OK and KED), the auto-correlation structures were modelled using a tide-dependent variogram. It is defined as a 3D horizontal variogram where the third dimension is the sea surface height anomaly (SHHa). The usual variograms are drawn in grey, yet they were not modeled and used for estimating abundance indices. Fitted models are shown in red.

Regarding Abundance indices, data characteristics (Table 1) reflected obviously on abundance indices estimations, with averaged AIs of 115.1×10^3, 18.7×10^3 and 42.3×10^3 individuals for years 2016 to 2018 respectively (Fig. 6). Abundance indices derived from random sampling were systematically smaller than other AIs, with AI twice higher with Transitive Kriging than with Random Sampling in 2018. Coefficient of variations were also way larger with kriging and particularly with Transitive Kriging. Indeed, Random Sampling methods led to CV of only 17 %, 18.5 % and 17.8 % for the three surveys respectively, while the best geostatistical approach estimated CVs of 33.5 %, 40.5 % and 46.1 %. However, for each survey, geostatistics methods had substantially better accuracy than random sampling techniques in the light of the cross-validation index; the RMSE (Fig. 6). Indeed, for each survey the lowest RMSE was obtained by either Transitive Kriging or Kriging with External Drift (Fig. 6). In particular, Kriging with External Drift had

the best results for two surveys (2016 and 2017), corresponding to surveys where we found a significant relationship between fish density and salinity Table 2. On the 2018 dataset, Kriging with External Drift did not improve much the Ordinary Kriging (Fig. 6). The associated drift model found indeed a relationship between fish density and depth, with a R-squared of 0.02 only 2. The Ordinary Kriging obtained lower scores than the Random Sampling in 2016 and 2017, and in both cases the use of external drift substantially improved the prediction accuracy of this approach.

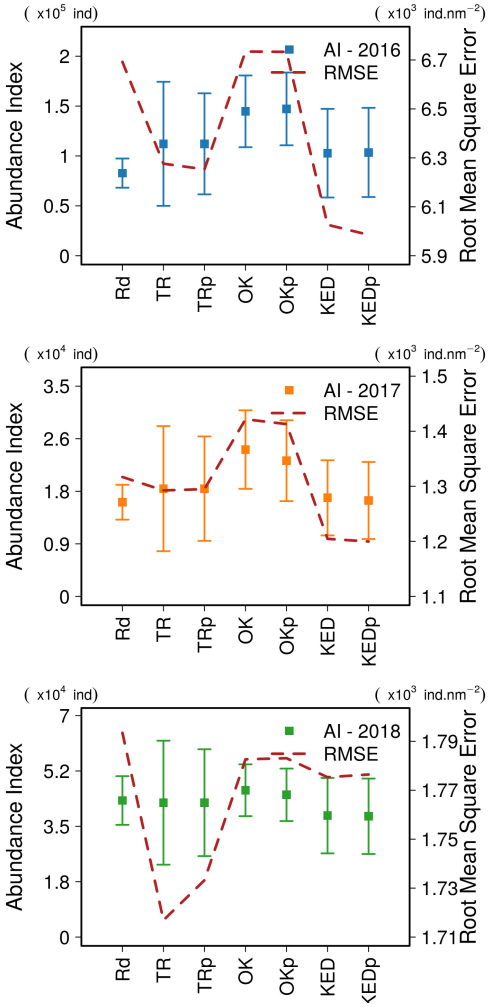

Figure 6: Index Abundance Estimation. Abundance estimations for each surveys and associated CVs are given for every models. Associated accuracy score is illustrated with dashed red lines representing the root mean squared error (RMSE) obtained through cross-validation

Maps produced by kriging methods also illustrated the inter-annual variability of fish juvenile densities (Fig.7). The highest fish densities were notably observed in the upstream part of the estuary in 2016 and 2017 whereas in 2018 they were relatively downstream (Table 1). Transitive approaches rendered relatively smooth maps with wide areas of medium densities, while Intrinsic kriging produced more constrated maps, revealing hotspots whose locations differed from one year to another. The use of external drift also induced important differences in the density distribution maps,

in particular by adding external information such as the location of the navigation channel (e.g. in 2018) and by accentuating the gradient of densities along the river bed with highest density upstream (e.g. in 2016 and 2017).

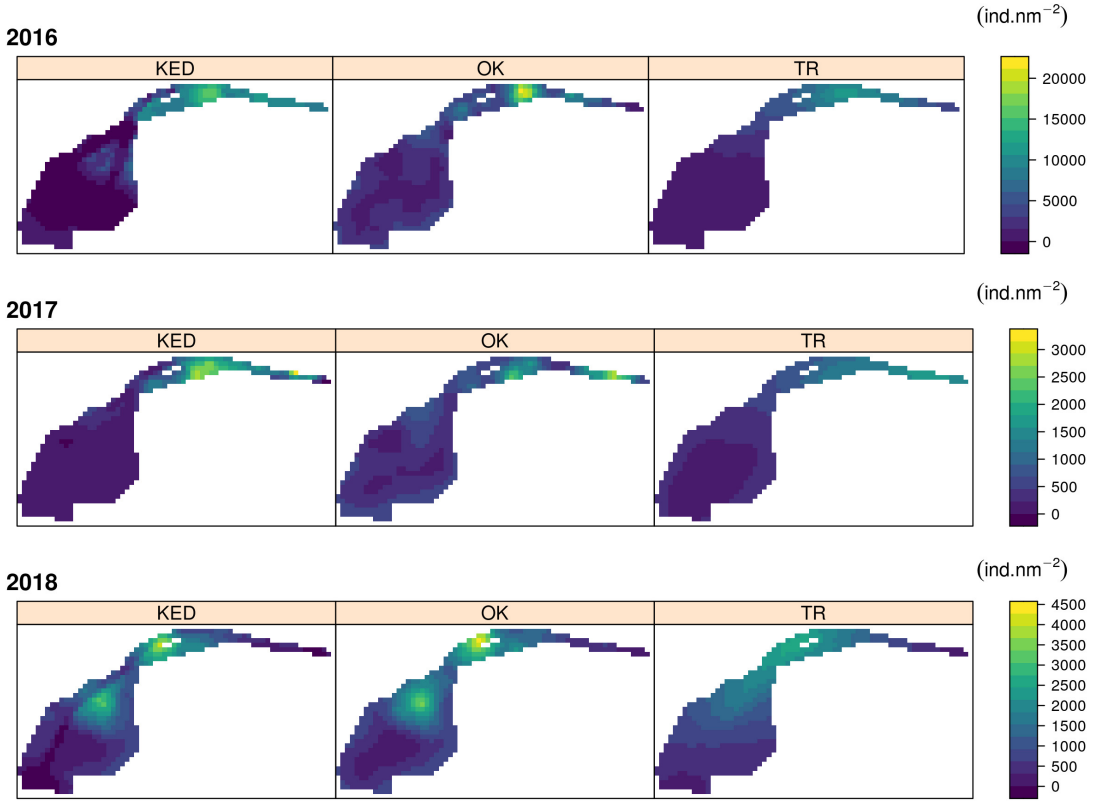

Figure 7: Kriged Maps of fish densities obtained for the same domain using different geostatistical methods over three distinct surveys. TR stands for transitive kriging, OK for ordinary kriging and KED for kriging with an external drift.

5 Discussion

Several studies have previously used geostatistics to estimate abundance indices of juvenile fishes in estuaries through Ordinary Kriging [45, 46, 47]. However, this sole focus on Ordinary Kriging might be misleading whenever the studied domains are non-convex and hold major environmental dynamics (i.e. the vast majority of estuaries) leading to clear violations of the underlying stationary hypothesis. In this study, we showed how the tidal movements of juveniles' sea bass increased the difficulty to estimate the spatial covariance structure of fish aggregations (Fig. 5), and that OK led to worse density predictions than the classic Random Sampling techniques in two of the three sampling years (Fig. 6). Therefore, the performance of OK will depend on both the shape and dynamics of the studied estuaries, but also on the behaviour of the studied fish in relation to water masses (size and swimming ability). For example, we might expect that groundfish would be less sensitive to tidal currents than demersal and pelagic fish (such as the sea bass), which would explain the quality of the variograms observed by [47]. It is therefore important to carefully evaluate the characteristics

of the focal estuary and species before using OK and alternative approaches should be carefully considered. Indeed, our study demonstrates how geostatistics can deal with these difficulties and yield to better abundance estimates than usual Random Sampling and Ordinary Kriging approaches (lower RMSE), notably with Transitive Kriging when no external data is available or by using Kriging with External Drift with spatio-temporal drifts that accounts for tidal dynamics and habitat preferendum.

Different metrics have been explored in the literature to describe spatial auto-correlations in estuaries such as the shortest distance over water [21, 20], the shortest temporal distance [48] or channel-centered coordinate transformation [49, 50]. Differences between kriging approaches with or without projection have been very subtle, yet it has facilitated considerably the interpretation of the variogram [49, 20]. In our case, we found that projection yielded most of the time to a better goodness of fit (Table 3 and Fig. 5). In particular, the estimation of anisotropy in a variogram is more natural within the channel-centered. The need of projection is however very specific to each estuary morphology and it might be difficult to assess general conclusions. As an alternative to the methods presented in this study, it is possible to deal with very irregularly-shaped estuarine and coastal environments with stochastic partial differential equations accounting for physical barriers [51] and implemented in R-INLA [52]. In this geostatistical framework, the fish densities are seen as the realization of a Gaussian random field which covariance structure is defined by some stochastic differential equation. The main idea is then to use a finite element approach to discretize the field and solve the equation with respect to sample observations.

The most striking result of our study is the substantial improvements of the models when time variability is taken into account (i.e. Kriging with External Drift in 2016 and 2017). Indeed, fish densities can vary substantially over short periods of time, and the sampling survey requires a certain amount of time. Such space-time interactions during a survey are known to be a difficulty for estimating a variogram from fish data [13]. Moreover, for practical reasons, surveys cannot always provide enough data for adding a third dimension and for estimating time variography such as proposed in [53]. A solution to deal with a time-series of surveys is to compute a mean variogram which can provide a more robust description of the spatial structure [54, 55]. In our case, the analysis of variography was particularly difficult since we had trawling stations at identical locations, but at different times. The estimation of a 3D variogram with sea surface height as third dimension enabled us to estimate a horizontal variogram selecting only pairs of positions with similar SSHa. Thus, we managed to capture a spatial auto-correlation structure (assumed constant through time), while no structure was observable using classical 2D variograms (Fig. 5). Then the idea consisted in kriging fish densities using a temporal drift to add a temporal effect without the need to estimate a temporal variogram, in the same way as performed previously for correcting daylight effects in abundance estimation of juvenile haddock [37]). By using salinity as external drift (i.e. a spatio-temporal variable that depend on the tides), our Kriging with External Drift accounted for tidal dynamics and outperforms other approaches on datasets from 2016 and 2017. Interestingly, we did not find any relevant drift in the 2018 dataset, and the best model had R-squared of only 0.02 (see Table 2). In this situation, using a drift was therefore useless and results were very similar to Ordinary Kriging. Other methods have used external data through GAMs [56, 57, 58], hierarchical Bayesian framework [59] or regression trees [60] but

without investigating spatial covariance structures. It would be interesting in a next step to compare geostatistics and these approaches but this is beyond the scope of this study.

This study focused on the inter-annual variability of distribution and abundance of 2-age juvenile seabass from Loire Estuary. The low number of 1-age juveniles captured in 2016 suggested indeed that G0- and G1-aged seabass could be difficult to capture, which would bias abundance estimation indices (see Fig. 3). This study confirms that the distributions of seabass juvenile are strongly related to tidal dynamics [29] and that the distribution and abundance within Loire's estuary were highly variable from one year to another (Fig. 7). This could be explained by major inter-annual variability in settlement timing and success of juvenile sea bass. Recent studies have indeed shown evidence of the impact of oceanographic features on the early life history phenology of seabass, with warmer waters delaying the hatching timing [61], with hydrological conditions (e.g. oceanographic currents, wind) influencing larvae drift and settlement success [62], and with food levels and starvation timing impacting larvae and juvenile survival [63]. The variability in the timing of juveniles recruitment in the nursery could explain that G2-aged sea bass sampled in the Loire estuary had different mean length and body condition between years. These morphological and potentially physiological differences could in turn lead to differences in their salinity preferendum, with a distribution of larger fish more downstream. The variability in settlement success could explain the particularly high estimated abundance in 2016 compared with 2017 and 2018. Further studies are clearly needed to tease apart settlement success and environmental conditions (e.g. flood in 2016) as the later may also have an impact on the estimates of abundance indices (e.g. fish availability). Indeed, juvenile sea bass are supposed to eventually disappear from shallow summer habitats during major flood as it might create local disruptions of habitat availability [7, 18].

Despite the variability of fish abundance for the three successive surveys, our study also revealed consistent influence of geostatistical method on AI estimates (Fig. 6). More specifically, all geostatistical methods had broadly similar AIs while RS was systematically smaller, which is related to the stratum design (Fig. 2). Indeed, the computation of AI through TR is similar to RS method in the particular case were there is one strata per sample position, consisting in the area of influence of every position. Moreover, the fact that the two best approaches TR, KED lead to similar AI supports the idea that using RS with an empirical stratum design can add a substantial bias in abundance estimations. Similarly, the OK obtained higher AIs than TR and KED in particular for years 2016-2017 where we observed evidence of relation between tidal dynamics and fish distributions (Fig. 3b). This suggests that the failure to comply with the stationarity hypothesis related to intrinsic geostatistics impact the estimation of AIs, and that methods such as KED or TR are needed to account for non-stationarity. In addition to the impact of geostatistical methods on AIs, the coefficients of variations (CVs) associated with these indices differed substantially between the RS and geostatistical approaches. More specifically, the geostatistical approaches had the best performances (lower RMSE) but were also associated to relatively high CVs compared with Random Sampling. This does not mean that RS is more accurate than geostatistical tools, but rather that ignoring spatial structure of dependence of samples and tidal effect leads to an overly optimistic precision. Indeed, the RS method fails at capturing accurately the high variance in observed densities at two nearby locations (in space and time). Moreover, the structure of the studied estuary with large stratas

downstream with few fishes and little variance (downstream) while small stratas contain all the variance (upstream) may lead therefore RS method to geometrically provide small CVs. Such underestimation of CVs associated to biases in AIs raises the relevance for the RS concerning the evaluation of juvenile abundance indices, and its consequences on the associated management actions. On the contrary, the Transitive approach managed to capture some spatial auto-correlation through its co-variogram with both low (hence better) goodness of fit and RMSE. CVs derived from TR were therefore the highest, as the variability of samples doubled at the same locations led to high nugget effects. This makes TR approaches particularly robust to non-stationarity and conservative for systematic abundance index estimations. Transitive and Intrinsic approaches also did not capture the same auto-correlation structure, the range of the modelled structures being higher using Transitive covariograms than using intrinsic variograms (see Table 3 and Fig. 5). By selecting only pairs of samples with similar SSHa, the intrinsic variogram observed indeed the averaged structure of fish densities at fixed time, while the transitive covariogram observed the structure of the averaged fish density through time. In other words, the covariogram captures the spatial structure of juvenile fish preferendum habitat, whereas the intrinsic variogram captures the fish schooling clusters structure. It is indeed observable in the kriged maps produced in Fig. 2 were TR-derived fish densities are way more smoothed than KED and OK maps. Estimated indices derived from TR and KED approaches were yet relatively similar as shown in Fig. 6 which once again supports the idea that TR is robust to tidal variability. KED would therefore be more relevant to investigate and explain the dynamics of fish densities along a tidal period, while TR provides a more pragmatic tool for stock management, as it captures well the averaged habitat structure of juvenile fishes, and allows the estimation of robust, unbiased and conservative abundance indices and maps, that could help designing protection areas.

In summary, our study shows how it is possible to use a wide variety of geostatistical methods to estimate juvenile fish abundance in nurseries. The versatility of these methods have thus far not really been considered in this context and such abundance indices (accurate, robust to environmental variability, having realistic CVs) should definitely be included in stock assessment models. This has already been done to some extent in the northern stock of the sea bass with the use of a simple densities average over ages 2-4 [64] but this can clearly be extended to other nurseries and to other approaches. Indeed, the use of geostatistically-computed abundance indices is a significant step towards a better estimation of fish abundances and an accurate estimation of their uncertainties. Compared to the classical random stratified estimators, geostatistics approaches are more conservative, but their higher uncertainties would allow a more robust adjustment trade-off between potentially different indices (i.e. estuaries) when estimating recruitment within a stock assessment model. Application of this general framework to any other fish stocks, whose juvenile life stage occurs in coastal nursery, might help the fisheries managers anticipating recruitment strength and better evaluating the consequences of alternative management actions.

Acknowledgements

The authors would like to thank all people involved in the surveys; Ronan Le Goff, Loïc Le Rû, Stéphane Martin, Didier Le Roy, Ludovic Bouché, Olivier Berthelé, François Garren, colleagues from the fishery biology laboratory

of Ifremer, Plouzané and Denis Bertho fisherman and owner of the Virgo Salutaris II. We are grateful to the team of the Sclerochronology Centre (Ifremer, Boulogne-sur-Mer, France), who estimate sea bass age from increment scale readings.

Funding statement

This study was part of the Nourdem project funded by the European Maritime and Fisheries Fund (EMFF-OSIRIS N°: PFEA 400018DM0310001), France Filière Pêche (FFP), the French Ministry of the Sea and Ifremer. Surveys have been conducted with the financial support of Bargip Nourriceries (2016): DPMA/FFP/Ifremer/CNPMEM, NourDem Loire (2017): FFP/CNPMEM/Ifremer, and NourDem Loire et Seine (2018): DPMA/CNPMEM/Ifremer.

Data availability

All data have been registered in the Harmonie database, which is available to those who request it on SIH website https://forms.ifremer.fr/sih/demande-de-donnees-aupres-du-sih/

References

1. Boehlert G and Mundy B. Roles of Behavioral and Physical Factors in Larval and Juvenile Fish Recruitment to Estuarine Nursery Areas. 1988 :17
2. Norcross BL and Shaw RF. Oceanic and Estuarine Transport of Fish Eggs and Larvae A Review. Transactions of the American Fisheries Society 1984; 113:153–65. DOI: 10.1577/1548-8659(1984)113<153:OAETOF>2.0.CO;2
3. Blaber SJM and Blaber TG. Factors Affecting the Distribution of Juvenile Estuarine and Inshore Fish. Journal of Fish Biology 1980; 17:143–62. DOI: 10/cvmvgw
4. Beck MW, Heck KL, Able KW, Childers DL, Eggleston DB, Gillanders BM, Halpern B, Hays CG, Hoshino K, Minello TJ, Orth RJ, Sheridan PF, and Weinstein MP. The Identification, Conservation, and Management of Estuarine and Marine Nurseries for Fish and Invertebrates. BioScience 2001; 51:633. DOI: 10/c487m2
5. Able KW. A Re-Examination of Fish Estuarine Dependence: Evidence for Connectivity between Estuarine and Ocean Habitats. Estuarine, Coastal and Shelf Science 2005; 64:5–17. DOI: 10/bndjmh
6. Dege M and Brown LR. Effect of Outflow on Spring and Summertime Distribution and Abundance of Larval and Juvenile Fishes in the Upper San Francisco Estuary. 2004 :18
7. Kelley D. Abundance, Growth and First-Winter Survival of Young Bass in Nurseries of South-West England. Journal of the Marine Biological Association of the United Kingdom 2002; 82:307–19. DOI: 10/dffjkn
8. Scharf FS. Patterns in Abundance, Growth, and Mortality of Juvenile Red Drum across Estuaries on the Texas Coast with Implications for Recruitment and Stock Enhancement. 2000 :16. DOI: 10/cjvkt8
9. Cochran WG. Sampling Techniques. New York, USA: John Wiley & Sons, 1977
10. Hankin DG and Reeves GH. Estimating Total Fish Abundance and Total Habitat Area in Small Streams Based on Visual Estimation Methods. Canadian Journal of Fisheries and Aquatic Sciences 1988; 45:834–44. DOI: 10.1139/f88-101
11. Rivoirard J, Simmonds J, Foote KG, Fernandes P, and Bez N. Geostatistics for Estimating Fish Abundance. Oxford: Blackwell Science Ltd, 2000
12. Matheron G. Estimating and Choosing: An Essay on Probability on Practice. Berlin: Springer-Verlag, 1989
13. Petitgas P. Geostatistics in Fisheries Survey Design and Stock Assessment: Models, Variances and Applications: Geostatistics for Fisheries Survey Design and Assessment. Fish and Fisheries 2001; 2:231–49. DOI: 10/fbghh9
14. Thorson JT, Shelton AO, Ward EJ, and Skaug HJ. Geostatistical Delta-Generalized Linear Mixed Models Improve Precision for Estimated Abundance Indices for West Coast Groundfishes. ICES Journal of Marine Science 2015; 72:1297–310. DOI: 10/f7gfxb
15. Shelton AO, Thorson JT, Ward EJ, and Feist BE. Spatial Semiparametric Models Improve Estimates of Species Abundance and Distribution. Canadian Journal of Fisheries and Aquatic Sciences 2014; 71. Ed. by Cooper A:1655–66. DOI: 10/ghsqhp

16. Bez N and Rivoirard J. Transitive Geostatistics to Characterise Spatial Aggregations with Diffuse Limits: An Application on Mackerel Ichtyoplankton. Fisheries Research 2001; 50:41–58. DOI: 10.1016/S0165-7836(00)00241-1

17. Laffaille P, Lefeuvre JC, Schricke MT, and Feunteun E. Feeding Ecology of 0-Group Sea Bass, Dicentrarchus Labrax, in Salt Marshes of Mont Saint Michel Bay (France). Estuaries 2001; 24:116. DOI: 10/d73gzr

18. Alp M and Pichon CL. Getting from Sea to Nurseries: Considering Tidal Dynamics of Juvenile Habitat Distribution and Connectivity in a Highly Modified Estuarine Riverscape. Ecosystems 2020. DOI: 10/gh5rwh

19. Martinho F, Leitão R, Neto JM, Cabral H, Lagardère F, and Pardal MA. Estuarine Colonization, Population Structure and Nursery Functioning for 0-Group Sea Bass (Dicentrarchus Labrax), Flounder (Platichthys Flesus) and Sole (Solea Solea) in a Mesotidal Temperate Estuary. Journal of Applied Ichthyology 2008; 24:229–37. DOI: 10/cgc5mp

20. Rathbun SL. Spatial Modelling in Irregularly Shaped Regions: Kriging Estuaries. Environmetrics 1998; 9:109–29. DOI: 10/b5w98r

21. Little LS, Edwards D, and Porter DE. Kriging in Estuaries: As the Crow Flies, or as the Fish Swims? Journal of Experimental Marine Biology and Ecology 1997; 213:1–11. DOI: 10/c8sjqm

22. Walmsley S, Bremner J, Walker A, Barry J, and Maxwell D. Challenges to Quantifying Glass Eel Abundance from Large and Dynamic Estuaries. ICES Journal of Marine Science 2018; 75. Ed. by Durif C:727–37. DOI: 10/gh278f

23. de Pontual H, Lalire M, Fablet R, Laspougeas C, Garren F, Martin S, Drogou M, and Woillez M. New Insights into Behavioural Ecology of European Seabass off the West Coast of France: Implications at Local and Population Scales. ICES Journal of Marine Science 2019; 76. Ed. by Grabowski J:501–15. DOI: 10.1093/icesjms/fsy08

24. ICES. Sea Bass (Dicentrarchus Labrax) in Divisions IVb-c, VIIa, and VII.d-h (Central and Southern North Sea, Irish Sea, English Channel, Bristol Channel, and Celtic Sea). ICES Advice on Fishing Opportunities, Catch, and Effort 2020. DOI: 10.17895/ices.advice.5916

25. López R, de Pontual H, Bertignac M, and Mahévas S. What Can Exploratory Modelling Tell Us about the Ecobiology of European Sea Bass (*Dicentrarchus Labrax*): A Comprehensive Overview. Aquatic Living Resources 2015; 28:61–79. DOI: 10/gh37qq

26. Martinho F, Leitão R, Neto JM, Cabral HN, Marques JC, and Pardal MA. The Use of Nursery Areas by Juvenile Fish in a Temperate Estuary, Portugal. Hydrobiologia 2007; 587:281–90. DOI: 10/dr8t66

27. Saillant E, Fostier A, Haffray P, Menu B, and Chatain B. Saline Preferendum for the European Sea Bass, Dicentrarchus Labrax, Larvae and Juveniles: Effect of Salinity on Early Development and Sex Determination. Journal of Experimental Marine Biology and Ecology 2003; 287:103–17. DOI: 10/bv3sc2

28. Green BC, Smith DJ, Grey J, and Underwood GJC. High Site Fidelity and Low Site Connectivity in Temperate Salt Marsh Fish Populations: A Stable Isotope Approach. Oecologia 2012; 168:245–55. DOI: 10/dxx7tm

29. Cabral H and Costa MJ. Abundance, Feeding Ecology and Growth of 0-Group Sea Bass, *Dicentrarchus Labrax* , within the Nursery Areas of the Tagus Estuary. Journal of the Marine Biological Association of the United Kingdom 2001; 81:679–82. DOI: 10/gh5sfq

30. Petitgas P, Woillez M, Rivoirard J, Renard D, and Bez N. Handbook of Geostatistics in R for Fisheries and Marine Ecology. ICES Cooperative Research Report 338. Copenhagen, Danmark: ICES, 2017 :177

31. Bez N and Braham CB. Indicator Variables for a Robust Estimation of an Acoustic Index of Abundance. Canadian Journal of Fisheries and Aquatic Sciences 2014; 71. Ed. by Jech JM:709–18. DOI: 10/gh2spq

32. Georgakarakos S and Kitsiou D. Mapping Abundance Distribution of Small Pelagic Species Applying Hydroacoustics and Co-Kriging Techniques. Hydrobiologia 2008; 612:155–69. DOI: 10/d38j9k

33. Lezama-Ochoa A, Ballón M, Woillez M, Grados D, Irigoien X, and Bertrand A. Spatial Patterns and Scale-Dependent Relationships between Macrozooplankton and Fish in the Bay of Biscay: An Acoustic Study. Marine Ecology Progress Series 2011; 439:151–68. DOI: 10/c3f5rq

34. Mesquita C, Dobby H, Pierce GJ, Jones CS, and Fernandes PG. Abundance and Spatial Distribution of Brown Crab (Cancer Pagurus) from Fishery-Independent Dredge and Trawl Surveys in the North Sea. ICES Journal of Marine Science 2020. Ed. by Hunsicker M:fsaa105. DOI: 10/gh2str

35. Woillez M, Rivoirard J, and Fernandes PG. Evaluating the Uncertainty of Abundance Estimates from Acoustic Surveys Using Geostatistical Simulations. ICES Journal of Marine Science 2009; 66:1377–83. DOI: 10/ccst2b

36. Chiles JP and Delfiner P. Geostatistics: Modeling Spatial Uncertainty. Vol. 497. John Wiley & Sons, 2009

37. Rivoirard J. Correcting for the Effect of Daylight in Abundance Estimation of Juvenile Haddock (Melanogrammus Aeglefinus) in the North Sea: An Application of Kriging with External Drift. ICES Journal of Marine Science 2001; 58:1272–85. DOI: 10.1006/jmsc.2001.1112

38. Drogou M, Le Goff R, Le Roy D, Martin S, Le Ru L, Bouche L, Roy A, Berthele O, and Lebigre C. Nourdem Loire et Nourdem Seine Bilan Des Campagnes 2018. Tech. rep. RST-RBE/STH 2019. Ifremer, 2019 :104

39. Le Goff R, Drogou M, Le Ru L, Garren F, Martin S, Bouche L, Le Roy D, and Berthele O. Nourdem Seine : bilan de la campagne 2017. Tech. rep. RST-RBE/STH/LBH 2017-001. Ifremer, 2017. DOI: 10.13155/52262

40. Gringarten E and Deutsch CV. Teacher's Aide Variogram Interpretation and Modeling. Mathematical Geology 2001 :28. DOI: 10/b7bgrj

41. Sahlin J, Mostafavi MA, Forest A, and Babin M. Assessment of 3D Spatial Interpolation Methods for Study of the Marine Pelagic Environment. Marine Geodesy 2014; 37:238–66. DOI: 10/gh2742

42. MINES ParisTech / ARMINES. RGeostats: The Geostatistical r Package. Fontainebleau, France, 2020

43. Desassis N and Renard D. Automatic Variogram Modeling by Iterative Least Squares: Univariate and Multivariate Cases. Mathematical Geosciences 2013; 45:453–70. DOI: 10/f4x4fx

44. Caillaud M, Petton S, Dumas F, Sebastien R, and Mickael V. Rejeu Hydrodynamique à 500 m de Résolution Avec Le Modèle MARS3D-AGRIF - Zone Manche-Gascogne. 2016. DOI: 10.12770/3EDEE80F-5A3E-42F4-9427-9684073C87F5

45. da Silva DR, Paranhos R, and Vianna M. Spatial Patterns of Distribution and the Influence of Seasonal and Abiotic Factors on Demersal Ichthyofauna in an Estuarine Tropical Bay: Ichthyofauna of Estuarine Tropical Bay. Journal of Fish Biology 2016; 89:821–46. DOI: 10/gh2s7b

46. Rueda M. Spatial Distribution of Fish Species in a Tropical Estuarine Lagoon: A Geostatistical Appraisal. Marine Ecology Progress Series 2001; 222:217–26. DOI: 10/ckk2n8

47. Tableau A, Brind'Amour A, Woillez M, and Le Bris H. Influence of Food Availability on the Spatial Distribution of Juvenile Fish within Soft Sediment Nursery Habitats. Journal of Sea Research 2016; 111:76–87. DOI: 10/f8sh9r

48. Zhang Y, Xian C, Chen H, Grieneisen ML, Liu J, and Zhang M. Spatial Interpolation of River Channel Topography Using the Shortest Temporal Distance. Journal of Hydrology 2016; 542:450–62. DOI: 10/f9ctrd

49. Legleiter CJ and Kyriakidis PC. Spatial Prediction of River Channel Topography by Kriging. Earth Surface Processes and Landforms 2008; 33:841–67. DOI: 10/bs5xxk

50. Goff JA and Nordfjord S. Interpolation of Fluvial Morphology Using Channel-Oriented Coordinate Transformation: A Case Study from the New Jersey Shelf. Mathematical Geology 2004; 36:643–58. DOI: 10/dj8nvj

51. Bakka H, Vanhatalo J, Illian J, Simpson D, and Rue H. Non-Stationary Gaussian Models with Physical Barriers. arXiv:1608.03787 [stat] 2019. arXiv: 1608.03787 [stat]

52. Lindgren F and Rue H. Bayesian Spatial Modelling with *R* - **INLA**. Journal of Statistical Software 2015; 63. DOI: 10/gdz6zz

53. Petitgas P. Sole Egg Distributions in Space and Time Characterised by a Geostatistical Model and Its Estimation Variance. ICES Journal of Marine Science 1997; 54:213–25. DOI: 10.1006/jmsc.1996.0184

54. Morfin M and Fromentin JM. Spatio-Temporal Patterns of Key Exploited Marine Species in the Northwestern Mediterranean Sea. PLoS ONE 2012; 7:14. DOI: 10/f3z22z

55. Saraux C, Fromentin JM, Bigot JL, Bourdeix JH, Morfin M, Roos D, Beveren EV, and Bez N. Spatial Structure and Distribution of Small Pelagic Fish in the Northwestern Mediterranean Sea. PLOS ONE 2014; 9:12. DOI: 10/ghw8zz

56. Hashimoto M, Nishijima S, Yukami R, Watanabe C, Kamimura Y, Furuichi S, Ichinokawa M, and Okamura H. Spatiotemporal Dynamics of the Pacific Chub Mackerel Revealed by Standardized Abundance Indices. Fisheries Research 2019; 219:105315. DOI: 10/ggkqt2

57. Polansky L, Newman KB, Nobriga ML, and Mitchell L. Spatiotemporal Models of an Estuarine Fish Species to Identify Patterns and Factors Impacting Their Distribution and Abundance. Estuaries and Coasts 2018; 41:572–81. DOI: 10/gcxwjp

58. Sobocinski KL, Ciannelli L, Wakefield WW, Yergey ME, and Johnson-Colegrove A. Distribution and Abundance of Juvenile Demersal Fishes in Relation to Summer Hypoxia and Other Environmental Variables in Coastal Oregon, USA. Estuarine, Coastal and Shelf Science 2018; 205:75–90. DOI: 10/gdvvwb

59. Rezende GA, Rufener MC, Ortega I, Ruas VM, and Dumont LFC. Modelling the Spatio-Temporal Bycatch Dynamics in an Estuarine Small-Scale Shrimp Trawl Fishery. Fisheries Research 2019; 219:105336. DOI: 10/gf8s6d

60. Froeschke JT and Froeschke BF. Spatio-Temporal Predictive Model Based on Environmental Factors for Juvenile Spotted Seatrout in Texas Estuaries Using Boosted Regression Trees. Fisheries Research 2011; 111:131–8. DOI: 10/fkwhfb

61. Pinto M, Monteiro J, Crespo D, Costa F, Rosa J, Primo A, Pardal M, and Martinho F. Influence of Oceanic and Climate Conditions on the Early Life History of European Seabass Dicentrarchus Labrax. Marine Environmental Research 2021; 169:105362. DOI: 10/gm425b

62. Beraud C, van der Molen J, Armstrong M, Hunter E, Fonseca L, and Hyder K. The Influence of Oceanographic Conditions and Larval Behaviour on Settlement Success—the European Sea Bass Dicentrarchus Labrax (L.) ICES Journal of Marine Science 2018; 75. Ed. by Kaplan D:455–70. DOI: 10/gm424g

63. Dambrine C, Huret M, Woillez M, Pecquerie L, Allal F, Servili A, and de Pontual H. Contribution of a Bioenergetics Model to Investigate the Growth and Survival of European Seabass in the Bay of Biscay – English Channel Area. Ecological Modelling 2020; 423:109007. DOI: 10/gm4244

64. Tidbury HJ, Muench A, Lamb PD, and Hyder K. Balancing Biological and Economic Goals in Commercial and Recreational Fisheries: Systems Modelling of Sea Bass Fisheries. ICES Journal of Marine Science 2021 :fsab087. DOI: 10/gj7g77

Annex

Table 3: Models Overview. An example of fitted model and associated empirical variograms is given in Fig. 5. Spherical range is detailed with two values when accounting for anisotropy.

Year	Kriging Approach	External Drift	Projection	Name	Nugget	Spherical Sill	Spherical Range	Goodness of fit
2016	Transitive	-	No	TR	0.078	0.06	15:5	0.61
		-	Yes	TRp	0.101	0.049	15:5	0.3
	Ordinary	No	No	OK	0.35	0.51	1.5	1.65
			Yes	OKp	0.33	0.5	1.5	1.2
		Yes	No	KED	0.95	0.15	1.5	1.27
			Yes	KEDp	0.9	0.2	1.5	1.2
2017	Transitive	-	No	TR	0.11	0.042	20:10	0.84
		-	Yes	TRp	0.099	0.032	15:5	0.25
	Ordinary	No	No	OK	0.37	0.42	2	2.54
			Yes	OKp	0.39	0.41	2	2.66
		Yes	No	KED	0.54	0.45	2	3.19
			Yes	KEDp	0.56	0.45	2	3.08
2018	Transitive	-	No	TR	0.069	0.027	15:10	0.49
		-	Yes	TRp	0.067	0.022	15:5	0.3
	Ordinary	No	No	OK	0.31	0.38	3	2.0
			Yes	OKp	0.32	0.37	3	1.96
		Yes	No	KED	0.34	0.33	3	1.74
			Yes	KEDp	0.34	0.32	3	1.82

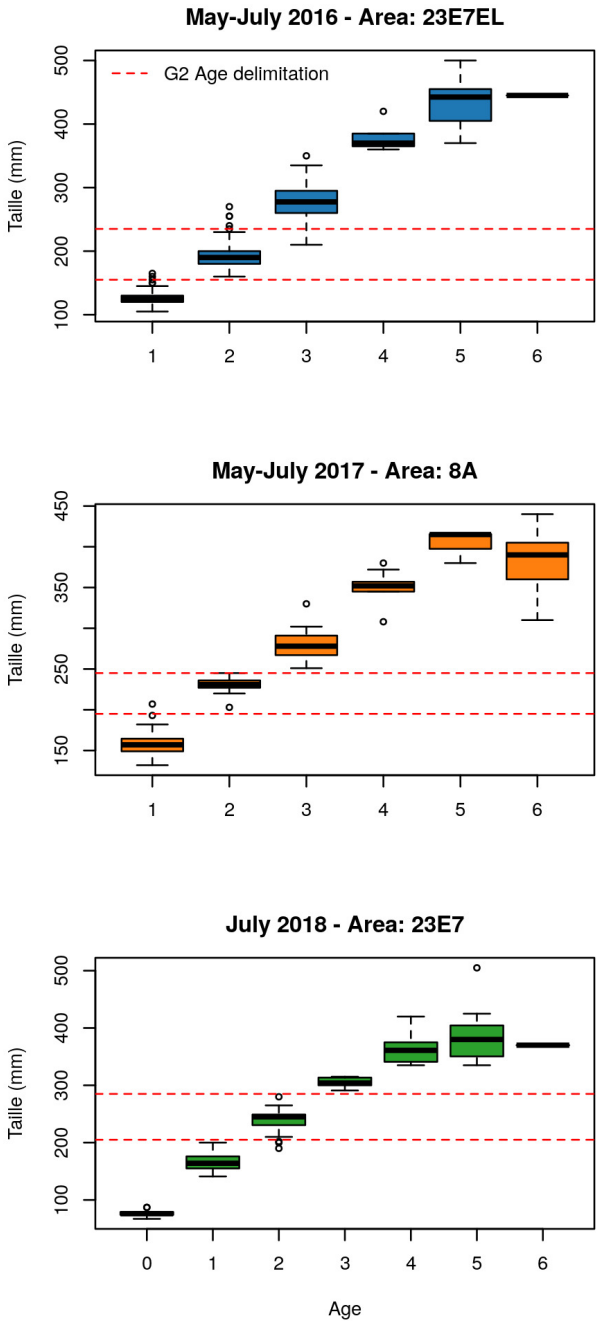

Figure 8: Age-length keys distribution based on increment scale readings sampled from The Nourdem surveys. Red dotted lines consist in the empirical delimitation used in the study.